Supplemental Material for "Higher-Order Weyl-Exceptional-Ring Semimetals"

Tao Liu,[1,*] James Jun He,[2,*] Zhongmin Yang,[1,3,4,†] and Franco Nori[5,6,7,‡]

[1]School of Physics and Optoelectronics, South China University of Technology, Guangzhou 510640, China
[2]RIKEN Center for Emergent Matter Science, Wako, Saitama 351-0198, Japan
[3]South China Normal University, Guangzhou 510006, China
[4]State Key Laboratory of Luminescent Materials and Devices and Institute of Optical Communication Materials, South China University of Technology, Guangzhou 510640, China
[5]Theoretical Quantum Physics Laboratory, RIKEN Cluster for Pioneering Research, Wako-shi, Saitama 351-0198, Japan
[6]RIKEN Center for Quantum Computing (RQC), Wako-shi, Saitama 351-0198, Japan
[7]Department of Physics, University of Michigan, Ann Arbor, Michigan 48109-1040, USA

I. HERMITIAN HIGHER-ORDER WEYL SEMIMETALS

As shown in the main text, we consider the following minimal Hamiltonian

$$\begin{aligned}\mathcal{H}(\mathbf{k}) = \;& \left(m_0 - \cos k_x - \cos k_y + m_1 \cos k_z\right) s_z\sigma_z + \left(v_z \sin k_z + i\gamma\right) s_z + \sin k_x s_x\sigma_z + \sin k_y s_y \sigma_z \\ & + \Delta_0 \left(\cos k_x - \cos k_y\right) \sigma_x, \end{aligned} \tag{S1}$$

In the absence of the non-Hermitian term (i.e., $\gamma = 0$), the Hermitian Hamiltonian $\mathcal{H}(\mathbf{k}, \gamma = 0)$ breaks the inversion symmetry $\mathcal{P}$, but preservers the time-reversal symmetry $\mathcal{T} = is_x\sigma_x\mathcal{K}$, with $\mathcal{K}$ being the complex conjugation operator. The eigenenergy $\mathcal{E}$ of the Hamiltonian for $\gamma = 0$ is

$$\mathcal{E}^2 = \left(|v_z \sin k_z| \pm \sqrt{\left(m_0 - \cos k_x - \cos k_y + m_1 \cos k_z\right)^2 + \Delta^2 \left(\cos k_x - \cos k_y\right)^2}\right)^2 + \sin^2 k_x + \sin^2 k_y. \tag{S2}$$

According to Eq. (S2), the Hermitian Hamiltonian supports higher-order Weyl nodes located at $(k_x,\ k_y,\ k_z) = (0,\ 0,\ k_w)$, where k_w satisfies

$$v_z^2 \sin^2 k_w \pm \left(m_0 - 2 + m_1 \cos k_w\right)^2 = 0. \tag{S3}$$

As shown in Fig. S1(a), there exist four Weyl nodes in momentum space, which are connected through surface Fermi arcs [see Fig. S1(b)] for the open boundary condition along the x direction. Moreover, when the boundaries along both the x and y directions are opened, hinge Fermi-arc states appear, which connect the two Weyl nodes closest to $k_z = 0$. Therefore, the Hermitian Hamiltonian $\mathcal{H}(\mathbf{k}, \gamma = 0)$ is a hybrid-order Weyl semimetal.

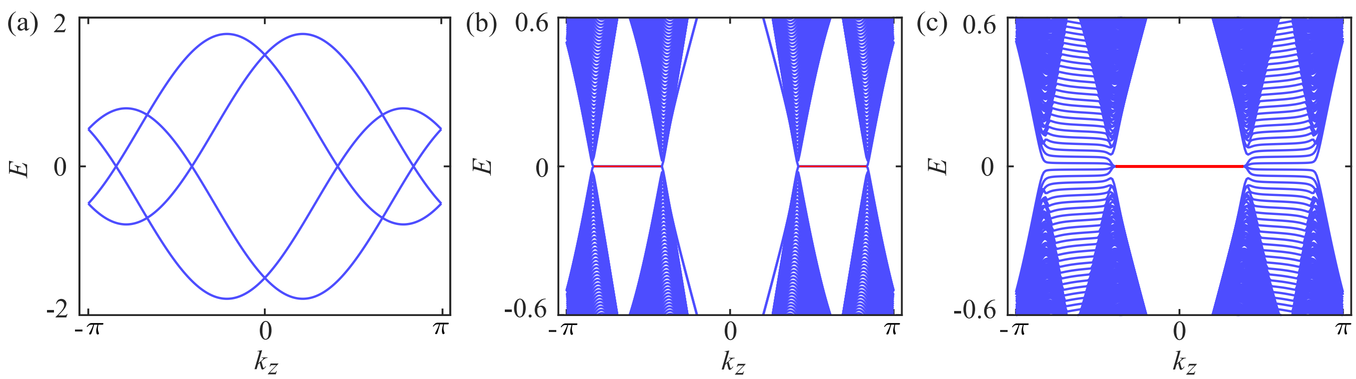

FIG. S1. (a) Bulk band structure along the k_z direction for $k_x = k_y = 0$. There exist four Weyl nodes, at which bulk bands are two-fold degenerate and eigenenergies are zero. (b) Surface band structure along the k_z direction under the open boundary condition along the x direction for $k_y = 0$. Two Weyl nodes located at the negative (positive) k_z axis are connected by surface Fermi arcs (red lines). (c) Band structure of a finite-sized system with 60×60 unit cells in the x-y plane. The hinge Fermi arcs (red lines) connect two Weyl nodes closest to $k_z = 0$, which are second-order Weyl nodes. The parameters used here are: $m_0 = 1.5$, $m_1 = -1$, $v_z = 0.8$, $\gamma = 0$, and $\Delta_0 = 0.8$.

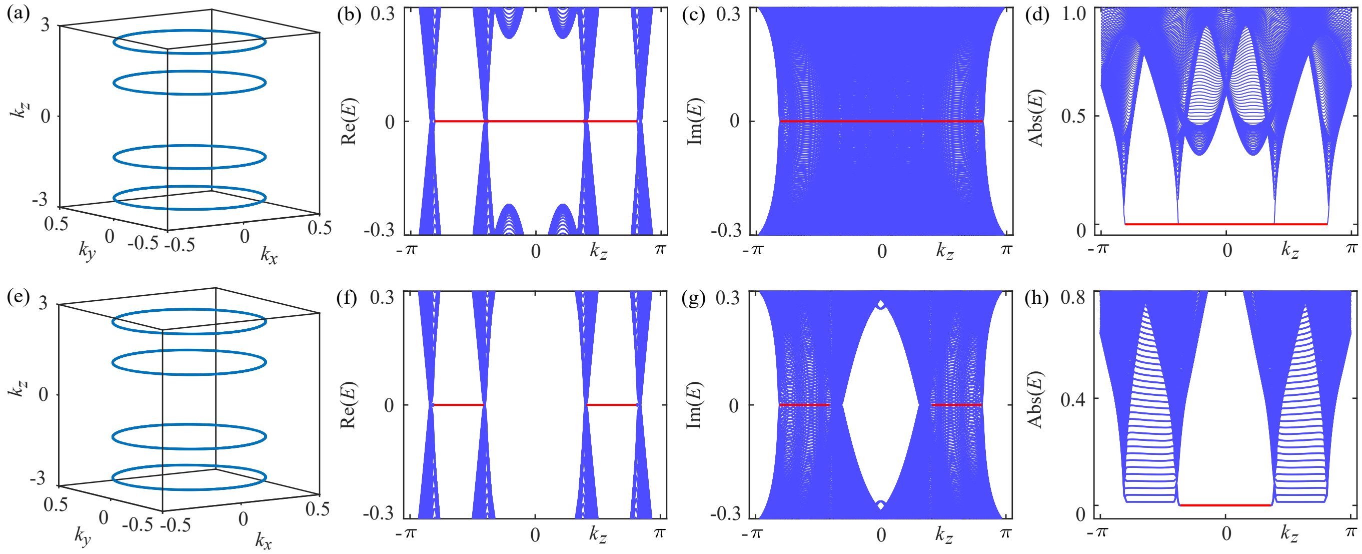

FIG. S2. First-order (first row) and higher-order (second row) topological semimetals for $\gamma = 0.4$. (a) Four Weyl exceptional rings along the k_z direction in the first-order topological semimetal for $\Delta_0 = 0$. (b) Real, (c) imaginary, and (d) absolute values of the surface band structure along the k_z direction for $\Delta_0 = 0$, when the open boundary condition is imposed along the x direction with 200 sites for $k_y = 0$. Note that only the modes with zero absolute energy are surface states (red lines). (e) Four Weyl exceptional rings along the k_z direction in the second-order topological semimetal for $\Delta_0 = 0.8$. (f) Real and (g) imaginary parts of the surface band structure along the k_z direction for $\Delta_0 = 0.8$, when the open boundary condition is imposed along the x direction with 200 sites for $k_y = 0$. (h) Absolute values of the band structure of a finite-sized system with 60×60 unit cells in the x-y plane. Note that only the modes with zero absolute energy are surface and hinge states (red lines). The common parameters used here are: $m_0 = 1.5$, $m_1 = -1$, $v_z = 0.8$, and $\gamma = 0.4$.

II. WEYL EXCEPTIONAL RINGS

In the presence of the non-Hermitian term, the eigenenergy E of the Hamiltonian $\mathcal{H}(\mathbf{k})$ can be written as

$$\begin{aligned} E^2 =& \left(m_0 - \cos k_x - \cos k_y + m_1 \cos k_z\right)^2 + \Delta^2 \left(\cos k_x - \cos k_y\right)^2 - \left(\gamma - i v_z \sin k_z\right)^2 + \sin^2 k_x + \sin^2 k_y \\ & \pm 2\left(i\gamma + v_z \sin k_z\right)\left[\left(m_0 - \cos k_x - \cos k_y + m_1 \cos k_z\right)^2 + \Delta^2 \left(\cos k_x - \cos k_y\right)^2\right]^{1/2} \end{aligned} \tag{S4}$$

To have the bands coalescence, we require $E^2 = 0$, namely,

$$\left(m_0 - \cos k_x - \cos k_y + m_1 \cos k_z\right)^2 + \Delta^2 \left(\cos k_x - \cos k_y\right)^2 = v_z^2 \sin^2 k_z, \tag{S5}$$

$$\left(|v_z \sin k_z| - \sqrt{\left(m_0 - \cos k_x - \cos k_y + m_1 \cos k_z\right)^2 + \Delta^2 \left(\cos k_x - \cos k_y\right)^2}\right)^2 + \sin^2 k_x + \sin^2 k_y = \gamma^2. \tag{S6}$$

In the above, without loss of generality, we have required $v_z > 0$. According to Eqs. (S5) and (S6), we have

$$\sin^2 k_x + \sin^2 k_y = \gamma^2, \tag{S7}$$

and

$$\left(m_0 - \cos k_x - \cos k_y + m_1 \cos k_z\right)^2 + \Delta^2 \left(\cos k_x - \cos k_y\right)^2 = v_z^2 \sin^2 k_z. \tag{S8}$$

III. EFFECTIVE SURFACE HAMILTONIAN IN THE GAPPED REGIMES

For $\Delta_0 = 0$, the Hamiltonian $\mathcal{H}(\mathbf{k})$ in Eq. (S1) is a first-order topological semimetal with the Weyl exceptional rings [see Fig. S2(a-d)], while the Δ_0 leads to a higher-order Weyl-exceptional-ring semimetal [see Fig. S2(e-h)]. Thus, the Δ_0 term

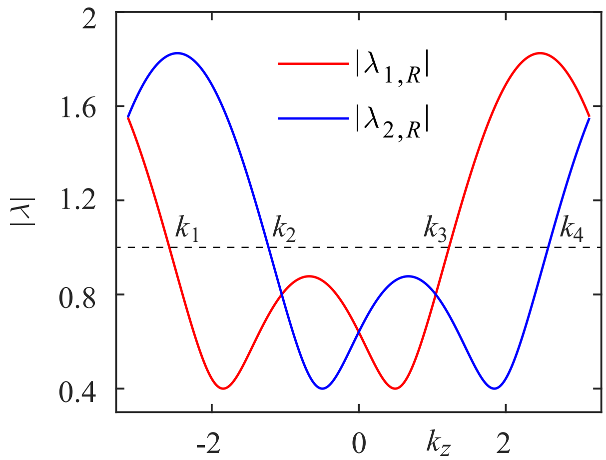

FIG. S3. $|\lambda_{1,R}|$ and $|\lambda_{2,R}|$ versus k_z, according to Eq. (S18), with $m_0 = 1.5$, $m_1 = -1$, $v_z = 0.8$, and $\gamma = 0.4$. The horizontal dashed black line denotes $|\lambda| = 1$, which is just guided for eyes. The projections of four exceptional rings of $\mathcal{H}_0$ are located at k_1, k_2, k_3 and k_4. As k_z increases from 0 to π (or decreases from 0 to $-\pi$), the non-Hermitian system $\mathcal{H}_0$ first supports two surface states localized for $k_2 < k_z < k_3$ at the boundary $x = 1$, and then only one surface state localized for $k_1 < k_z < k_2$ or $k_3 < k_z < k_4$ at the boundary as $|k_z|$ exceeds a critical value (i.e., k_2 and k_3).

gaps out the surface bands in the finite k_z region in the first Brillouin zone. In this part, we derive the low-energy effective Hamiltonians of surface bands in the gapped bulk-band regime for the relatively small γ and Δ_0. We label the four surfaces of a cubic sample as I, II, III, IV, corresponding to the boundary states localized at $x = 1$, $y = 1$, $x = L$, and $y = L$.

We first consider the system under open boundary condition along the x direction, and periodic boundary conditions along both the y and z directions. After a partial Fourier transformation along the k_x direction, the Hamiltonian $\mathcal{H}(\mathbf{k})$ in Eq. (S1) becomes

$$\begin{aligned}\mathcal{H}_x(k_y,\ k_z) = & \sum_{x,k_y,k_z} \Psi^{\dagger}_{x,k_y,k_z} \left[(m_0 - \cos k_y + m_1 \cos k_z) s_z \sigma_z + (v_z \sin k_z + i\gamma) s_z + \sin k_y s_y \sigma_z \right. \\ & \left. - \Delta_0 \cos k_y \sigma_x \right] \Psi_{x,k_y,k_z} + \sum_{x,k_y,k_z} \left[\Psi^{\dagger}_{x,k_y,k_z} \left(-\frac{1}{2} s_z \sigma_z - \frac{i}{2} s_x \sigma_z + \frac{\Delta_0}{2} \sigma_x \right) \Psi_{x+1,k_y,k_z} + \text{H.c.} \right], \end{aligned} \tag{S9}$$

where x is the integer-valued coordinate taking values from 1 to L, and $\Psi^{\dagger}_{x,k_y,k_z}$ creates a fermion with spin and orbital degrees of freedom on site x and momentum k_y and k_z. By assuming a small Δ_0 and taking k_y to be close to 0, we rewrite $\mathcal{H}_x$ as $\mathcal{H}_x = \mathcal{H}_0 + \mathcal{H}_1$, with

$$\mathcal{H}_0 = \sum_{x,k_y,k_z} \Psi^{\dagger}_{x,k_y,k_z} M \Psi_{x,k_y,k_z} + \sum_{x,k_y,k_z} \left(\Psi^{\dagger}_{x,k_y,k_z} T \Psi_{x+1,k_y,k_z} + \text{H.c.} \right), \tag{S10}$$

where $M = (m_0 - \cos k_y + m_1 \cos k_z) s_z \sigma_z + (v_z \sin k_z + i\gamma) s_z$, and $T = -\frac{1}{2} s_z \sigma_z - \frac{i}{2} s_x \sigma_z$, and

$$\mathcal{H}_1 = \sum_{x,k_y,k_z} \Psi^{\dagger}_{x,k_y,k_z} (\sin k_y s_y \sigma_z - \Delta_0 \cos k_y \sigma_x) \Psi_{x,k_y,k_z} + \sum_{x,k_y,k_z} \left(\Psi^{\dagger}_{x,k_y,k_z} \frac{\Delta_0}{2} \sigma_x \Psi_{x+1,k_y,k_z} + \text{H.c.} \right), \tag{S11}$$

where $\mathcal{H}_1$ is treated as a perturbation.

Since the Hamiltonian $\mathcal{H}_0$ in Eq. (S10) is non-Hermitian, we calculate its left and right eigenstates. We first solve the right eigenstates. In order to solve the surface states localized at the boundary $x = 1$, we choose a trial solution $\psi_R(x) = \lambda_R^x \phi_R$, where λ_R is a parameter determining the localization length with $|\lambda_R| < 1$, and ϕ_R is a four-component vector. Plugging this trial solution into Hamiltonian $\mathcal{H}_0$ in Eq. (S10) for $k_y = 0$, we have the following eigenvalue equations:

$$\left(\lambda_R^{-1} T^{\dagger} + M + \lambda_R T \right) \phi_R = E \phi_R, \qquad \text{in the bulk,} \tag{S12}$$

and

$$(M + \lambda_R T) \phi_R = E \phi_R, \qquad \text{at the boundary } x = 1. \tag{S13}$$

By considering the semi-infinite limit $L \to \infty$, and requiring the states have the same eigenenergy in the bulk and at the boundary, we have $\lambda_R^{-1} T^\dagger \phi_R = 0$. This leads to $E = 0$, and two corresponding eigenstates $\psi_{1,R}$ and $\psi_{2,R}$. The eigenstate $\psi_{1,R}$ is written as

$$\psi_{1,R} = \mathcal{N}_1 (\lambda_{1,R}\phi_{1,R},\ \lambda_{1,R}^2\phi_{1,R},\ \lambda_{1,R}^3\phi_{1,R},\ \dots), \tag{S14}$$

with

$$\phi_{1,R} = (-i,\ 0,\ 1,\ 0)^T, \quad \text{and} \quad \lambda_{1,R} = 1 - m_0 - m_1 \cos k_z - v_z \sin k_z - i\gamma. \tag{S15}$$

The eigenstate $\psi_{2,R}$ is

$$\psi_{2,R} = \mathcal{N}_2 (\lambda_{2,R}\phi_{2,R},\ \lambda_{2,R}^2\phi_{2,R},\ \lambda_{2,R}^3\phi_{2,R},\ \dots), \tag{S16}$$

with

$$\phi_{2,R} = (0,\ -i,\ 0,\ 1)^T, \quad \text{and} \quad \lambda_{2,R} = 1 - m_0 - m_1 \cos k_z + v_z \sin k_z + i\gamma. \tag{S17}$$

For the surface states localized at the boundary $x = 1$, we require $|\lambda_{1,R}| < 1$ and $|\lambda_{2,R}| < 1$, then we have

$$\left[(1 - m_0 - m_1 \cos k_z - v_z \sin k_z)^2 + \gamma^2\right]^{1/2} < 1, \quad \text{and} \quad \left[(1 - m_0 - m_1 \cos k_z + v_z \sin k_z)^2 + \gamma^2\right]^{1/2} < 1. \tag{S18}$$

According to Eq. (S18), as k_z increases from 0 to π (or decreases from 0 to $-\pi$), the non-Hermitian system $\mathcal{H}_0$ first supports two surface states localized at the boundary $x = 1$, and then only one surface state as $|k_z|$ exceeds a critical value (i.e., one of exceptional points at which a phase transition takes place). As shown in Fig. S3, two surface states exist only in a finite region of k_z inbetween two exceptional rings closest to $k_z = 0$ for small γ. A surface energy gap, or a mass term, can exist only when two surface eigenstates coexist. Thus, the hinge states, regarded as boundary states between domains of opposite masses, appear only in a finite range of k_z.

We now proceed to solve the left eigenstates with a trial solution $\psi_L(x) = \lambda_L^x \phi_L$. As the same procedure for deriving the right eigenstates, we have the following eigenvalue equations:

$$\left(\lambda_L^{-1} T^\dagger + M^\dagger + \lambda_L T\right) \phi_L = E\phi_L, \quad \text{in the bulk}, \tag{S19}$$

and

$$\left(M^\dagger + \lambda_L T\right) \phi_L = E\phi_L, \quad \text{at the boundary } x = 1. \tag{S20}$$

By considering the semi-infinite limit, we have $E = 0$, and two corresponding eigenstates $\psi_{1,L}$ and $\psi_{2,L}$. The eigenstate $\psi_{1,L}$ is written as

$$\psi_{1,L} = \mathcal{N}_1^* (\lambda_{1,L}\phi_{1,L},\ \lambda_{1,L}^2\phi_{1,L},\ \lambda_{1,L}^3\phi_{1,L},\ \dots), \tag{S21}$$

with

$$\phi_{1,L} = (-i,\ 0,\ 1,\ 0)^T, \quad \text{and} \quad \lambda_{1,L} = 1 - m_0 - m_1 \cos k_z - v_z \sin k_z + i\gamma. \tag{S22}$$

The eigenstate $\psi_{2,L}$ is

$$\psi_{2,L} = \mathcal{N}_2^* (\lambda_{2,L}\phi_{2,L},\ \lambda_{2,L}^2\phi_{2,L},\ \lambda_{2,L}^3\phi_{2,L},\ \dots), \tag{S23}$$

with

$$\phi_{2,L} = (0,\ -i,\ 0,\ 1)^T, \quad \text{and} \quad \lambda_{2,L} = 1 - m_0 - m_1 \cos k_z + v_z \sin k_z - i\gamma. \tag{S24}$$

In Eqs. (S14, S16, S21, S23), the constants $\mathcal{N}_1$ and $\mathcal{N}_2$ are solved by biorthogonal conditions as

$$\mathcal{N}_1 = \sqrt{\left(1 - \lambda_{1,L}^* \lambda_{1,R}\right) / \left(2\lambda_{1,L}^* \lambda_{1,R}\right)}, \tag{S25}$$

$$\mathcal{N}_2=\sqrt{\left(1-\lambda_{1,L}^*\lambda_{1,R}\right)/\left(2\lambda_{1,L}^*\lambda_{1,R}\right)}. \tag{S26}$$

For the k_z region where the system supports two surface states, projecting the Hamiltonian $\mathcal{H}_1$ in Eq. (S11) into the subspace spanned by the above left and right eigenstates as $\mathcal{H}^{\rm I}_{\text{surf},\alpha\beta}=\psi^*_{\alpha,L}\mathcal{H}_1\psi_{\beta,R}$, we have the effective boundary Hamiltonian in the surface I as

$$\mathcal{H}^{\rm I}_{\text{surf,x}}(k_y,k_z)=k_y\sigma_z-(\eta-\xi)\,\sigma_x, \tag{S27}$$

where we have ignored the terms of order higher than k_y, and η and ξ are given by

$$\eta=2\Delta_0\mathcal{N}_1\mathcal{N}_2\lambda_{1,R}\lambda_{2,R}/\left(1-\lambda_{1,R}\lambda_{2,R}\right), \tag{S28}$$

$$\xi=\Delta_0\mathcal{N}_1\mathcal{N}_2\lambda_{1,R}\lambda_{2,R}\left(\lambda_{1,R}+\lambda_{2,R}\right)/\left(1-\lambda_{1,R}\lambda_{2,R}\right). \tag{S29}$$

When the system is under open boundary condition along the y direction, and periodic boundary conditions along both the x and z directions, after a partial Fourier transformation along the k_y direction, the Hamiltonian $\mathcal{H}(\mathbf{k})$ in Eq. (S1) becomes

$$\begin{aligned}\mathcal{H}_y(k_x,\ k_z)=&\sum_{y,k_x,k_z}\Psi^\dagger_{y,k_x,k_z}\left[\left(m_0-\cos k_x+m_1\cos k_z\right)s_z\sigma_z+\left(v_z\sin k_z+i\gamma\right)s_z+\sin k_x s_x\sigma_z\right.\\&\left.+\Delta_0\cos k_x\sigma_x\right]\Psi_{y,k_x,k_z}+\sum_{y,k_x,k_z}\left[\Psi^\dagger_{y,k_x,k_z}\left(-\frac{1}{2}s_z\sigma_z-\frac{i}{2}s_y\sigma_z-\frac{\Delta_0}{2}\sigma_x\right)\Psi_{y+1,k_x,k_z}+\text{H.c.}\right],\end{aligned} \tag{S30}$$

where y is an integer-valued coordinate taking values from 1 to L. By assuming a small Δ_0, and taking k_x to be close to 0, we rewrite $\mathcal{H}_y$ as $\mathcal{H}_y=\tilde{\mathcal{H}}_0+\tilde{\mathcal{H}}_1$, with

$$\tilde{\mathcal{H}}_0=\sum_{y,k_x,k_z}\Psi^\dagger_{y,k_x,k_z}\tilde{M}\Psi_{y,k_x,k_z}+\sum_{y,k_x,k_z}\left(\Psi^\dagger_{y,k_x,k_z}\tilde{T}\Psi_{y+1,k_x,k_z}+\text{H.c.}\right), \tag{S31}$$

where $\tilde{M}=\left(m_0-\cos k_x+m_1\cos k_z\right)s_z\sigma_z+\left(v_z\sin k_z+i\gamma\right)s_z$, and $\tilde{T}=-\frac{1}{2}s_z\sigma_z-\frac{i}{2}s_y\sigma_z$, and

$$\tilde{\mathcal{H}}_1=\sum_{y,k_x,k_z}\Psi^\dagger_{y,k_x,k_z}\left(\sin k_x s_x\sigma_z+\Delta_0\cos k_x\sigma_x\right)\Psi_{y,k_x,k_z}-\sum_{y,k_x,k_z}\left(\Psi^\dagger_{y,k_x,k_z}\frac{\Delta_0}{2}\sigma_x\Psi_{y+1,k_x,k_z}+\text{H.c.}\right). \tag{S32}$$

where $\tilde{\mathcal{H}}_1$ is treated as a perturbation. We first solve the right eigenstates. In order to solve the surface states localized at the boundary $y=L$, we choose a trial solution $\tilde{\psi}_R(y)=\tilde{\lambda}^y_R\tilde{\phi}_R$, where $\tilde{\lambda}$ is a parameter determining the localization length with $\left|\tilde{\lambda}_R\right|>1$, and $\tilde{\phi}_R$ is a four-component vector. Plugging this trial solution into the Hamiltonian $\tilde{\mathcal{H}}_0$ in Eq. (S31) for $k_x=0$, we have the following eigenvalue equations:

$$\left(\tilde{\lambda}_R^{-1}\tilde{T}^\dagger+\tilde{M}+\tilde{\lambda}_R\tilde{T}\right)\tilde{\phi}_R=E\tilde{\phi}_R,\quad\text{in the bulk}, \tag{S33}$$

and

$$\left(\tilde{\lambda}_R^{-1}\tilde{T}^\dagger+\tilde{M}\right)\tilde{\phi}_R=E\tilde{\phi}_R,\quad\text{at the boundary } y=L. \tag{S34}$$

By considering the semi-infinite limit along the y-axis in a negative direction, and requiring the states have the same eigenenergies in the bulk and at the boundary, we have $\tilde{\lambda}_R\tilde{T}=0$, which leads to $E=0$, and two corresponding eigenstates $\tilde{\psi}_{1,R}$ and $\tilde{\psi}_{2,R}$. The eigenstate $\tilde{\psi}_{1,R}$ is written as

$$\tilde{\psi}_{1,R}=\tilde{\mathcal{N}}_1(\tilde{\lambda}_{1,R}\tilde{\phi}_{1,R},\ \tilde{\lambda}^2_{1,R}\tilde{\phi}_{1,R},\ \tilde{\lambda}^3_{1,R}\tilde{\phi}_{1,R},\ \ldots), \tag{S35}$$

with

$$\tilde{\phi}_{1,R}=(1,\ 0,\ 1,\ 0)^T,\ \text{ and }\ \tilde{\lambda}_{1,R}=1/\left(1-m_0-m_1\cos k_z-v_z\sin k_z-i\gamma\right), \tag{S36}$$

and the eigenstate $\tilde{\psi}_{2,R}$ is

$$\tilde{\psi}_{2,R}=\tilde{\mathcal{N}}_2(\tilde{\lambda}_{2,R}\tilde{\phi}_{2,R},\ \tilde{\lambda}^2_{2,R}\tilde{\phi}_{2,R},\ \tilde{\lambda}^3_{2,R}\tilde{\phi}_{2,R},\ \ldots), \tag{S37}$$

with

$$\tilde{\phi}_{2,R} = (0,\ 1,\ 0,\ 1)^T, \ \text{ and } \ \tilde{\lambda}_{2,R} = 1/\left(1 - m_0 - m_1 \cos k_z + v_z \sin k_z + i\gamma\right), \tag{S38}$$

here $\lambda_{1,R} = 1/\tilde{\lambda}_{1,R}$ and $\lambda_{2,R} = 1/\tilde{\lambda}_{2,R}$. For the surface states localized at the boundary $y = L$, we require $\left|\tilde{\lambda}_{1,R}\right| > 1$ and $\left|\tilde{\lambda}_{2,R}\right| > 1$, then we have

$$\left[(1 - m_0 - m_1 \cos k_z - v_z \sin k_z)^2 + \gamma^2\right]^{1/2} < 1, \ \text{ and } \ \left[(1 - m_0 - m_1 \cos k_z + v_z \sin k_z)^2 + \gamma^2\right]^{1/2} < 1. \tag{S39}$$

According to Eq. (S39), as k_z increases from 0 to π (or decreases from 0 to $-\pi$), the non-Hermitian system $\mathcal{H}_0$ first supports two surface states localized at the boundary $y = L$, and then only one surface state localized at the boundary as $|k_z|$ exceeds a critical value (i.e., one of exceptional points at which a phase transition takes place). The critical values of k_z correspond to ones at which two exceptional rings closest to $k_z = 0$ locate for the case of small γ. Because the domain-wall states, as discussed below, only appear if $\mathcal{H}_0$ supports two surface states, the hinge Fermi-arc states exist only for a finite regime of k_z.

For the left eigenstates under the open boundary condition along the y direction, we assume a trial solution $\tilde{\psi}_L(y) = \tilde{\lambda}_L^y \tilde{\phi}_L$. Considering the same procedure for deriving the right eigenstates, we obtain the left eigenstates $\tilde{\psi}_{1,L}$ and $\tilde{\psi}_{2,L}$ as

$$\tilde{\psi}_{1,L} = \tilde{\mathcal{N}}_1^* (\tilde{\lambda}_{1,L}\tilde{\phi}_{1,L},\ \tilde{\lambda}_{1,L}^2\tilde{\phi}_{1,L},\ \tilde{\lambda}_{1,L}^3\tilde{\phi}_{1,L},\ \ldots), \tag{S40}$$

with

$$\tilde{\phi}_{1,L} = (1,\ 0,\ 1,\ 0)^T, \ \text{ and } \ \tilde{\lambda}_{1,L} = 1/\left(1 - m_0 - m_1 \cos k_z - v_z \sin k_z + i\gamma\right), \tag{S41}$$

and

$$\tilde{\psi}_{2,L} = \tilde{\mathcal{N}}_2^* (\tilde{\lambda}_{2,L}\tilde{\phi}_{2,L},\ \tilde{\lambda}_{2,L}^2\tilde{\phi}_{2,L},\ \tilde{\lambda}_{2,L}^3\tilde{\phi}_{2,L},\ \ldots), \tag{S42}$$

with

$$\tilde{\phi}_{2,L} = (0,\ 1,\ 0,\ 1)^T, \ \text{ and } \ \tilde{\lambda}_{2,L} = 1/\left(1 - m_0 - m_1 \cos k_z + v_z \sin k_z - i\gamma\right), \tag{S43}$$

For the k_z region where the system supports two surface states, projecting the Hamiltonian $\tilde{\mathcal{H}}_1$ in Eq. (S32) into the subspace spanned by the above right and left eigenstates as $\mathcal{H}^{\text{IV}}_{\text{surf},\alpha\beta} = \tilde{\psi}^*_{\alpha,L}\tilde{\mathcal{H}}_1\tilde{\psi}_{\beta,R}$, we have the effective boundary Hamiltonian in the surface IV

$$\mathcal{H}^{\text{IV}}_{\text{surf,y}}(k_x, k_z) = k_x\sigma_z + (\eta - \xi)\,\sigma_x, \tag{S44}$$

where we have ignored the terms of order higher than k_x.

By using the same procedure above, we have the effective Hamiltonian for boundary states localized at surfaces II and III as

$$\mathcal{H}^{\text{II}}_{\text{surf,y}}(k_x, k_z) = -k_x\sigma_z + (\eta - \xi)\,\sigma_x, \tag{S45}$$

$$\mathcal{H}^{\text{III}}_{\text{surf,x}}(k_y, k_z) = -k_y\sigma_z - (\eta - \xi)\,\sigma_x. \tag{S46}$$

According to the surface Hamiltonians in Eqs. (S27) and (S44-S46), as well as the condition in Eq. (S18), the surface states, in the gapped regime and a finite k_z region, show the same kinetic energy coefficients, but the mass terms on two neighboring surfaces always have opposite signs. Therefore, the mass domain walls appear at the intersection of two neighboring surfaces, and these two surfaces can share a common zero-energy boundary state (analogous to the Jackiw-Rebbi zero modes [1]) in spite of complex-valued μ, which corresponds to the hinge Fermi-arc states at each k_z. Moreover, these hinge Fermi-arc states exist only in a finite k_z region limited by the condition in Eq. (S18). This explains why the Hamiltonian $\mathcal{H}(\mathbf{k})$ shows both first-order and higher-order topological features for small γ.

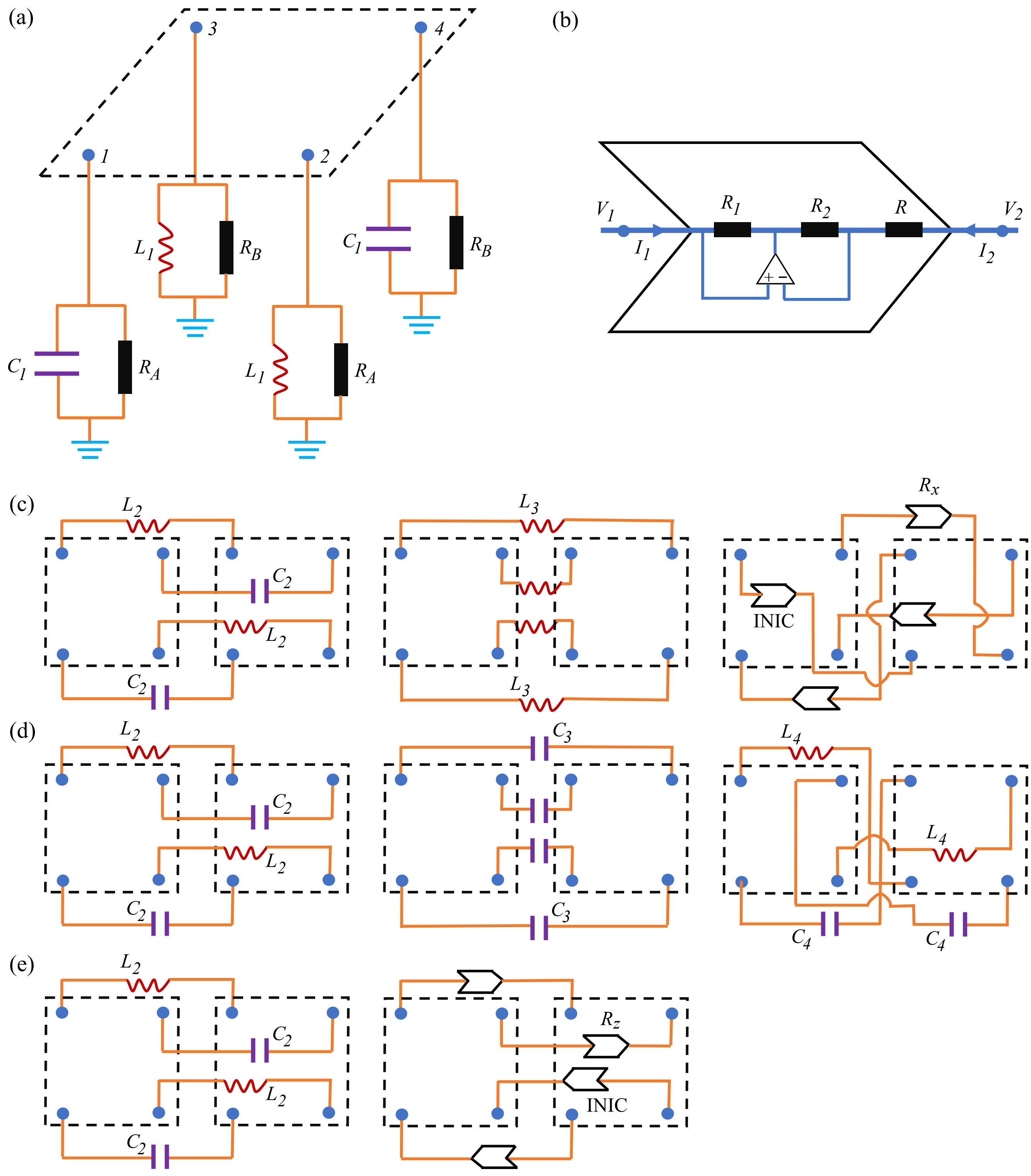

FIG. S4. (a) Schematic diagram of a unit cell of a cubic lattice realized by electric circuits. The unit-cell electric circuits consist of four nodes, and each node is connected to grounded electric elements for simulating the diagonal entries in the Hamiltonian $\mathcal{H}_1(x,\ y,\ z)$. The on-site gain and loss are realized by resistive elements R_A and R_B. C_1 and L_1 denote capacitances and inductances. (b) Negative impedance converter with current inversion (INIC) used for the hopping with imaginary amplitudes. (c-e) Diagrams of the electric circuits for simulating Hamiltonians $\mathcal{H}_2(x,\ y,\ z)$, $\mathcal{H}_3(x,\ y,\ z)$, and $\mathcal{H}_4(x,\ y,\ z)$, respectively. Here, C_2, C_3 and C_4 are capacitances, L_2, L_3 and L_4 denote inductances, R_x and R_z represent resistances of INICs.

IV. POSSIBLE EXPERIMENTAL REALIZATIONS USING TOPOELECTRIC CIRCUITS

Recently, non-Hermitian first-order and higher-order topological insulators [2, 3], 3D Hermitian higher-order topological insulators [4] and topological semimetals [5] have been experimentally observed in topoelectric circuits. These indicate that electric circuits are excellent platforms to realize complicated and exotic topological structures. In this section, we propose to realize the lattice model in Eq. (1) in the main text using topoelectric circuits. Without loss of generality, we set $m_1 = -1$, $m_0 > 0$, $v_z > 0$ and $\gamma > 0$.

The real-space Hamiltonian $\mathcal{H}(x,\ y,\ z)$ for Eq. (1) in the main text reads $\mathcal{H}(x,\ y,\ z) = \mathcal{H}_1(x,\ y,\ z) + \mathcal{H}_2(x,\ y,\ z) + \mathcal{H}_3(x,\ y,\ z) + \mathcal{H}_4(x,\ y,\ z)$, where

$$\mathcal{H}_1(x,\ y,\ z) = \sum_{x,y,z} \Psi^{\dagger}_{x,y,z} \left(m_0 s_z \sigma_z + i\gamma s_z\right) \Psi_{x,y,z}, \tag{S47}$$

$$\mathcal{H}_2(x,\ y,\ z) = \sum_{x,y,z} \left[\Psi^{\dagger}_{x,y,z} \left(-\frac{1}{2} s_z \sigma_z - \frac{i}{2} s_x \sigma_z + \frac{\Delta_0}{2}\sigma_x\right) \Psi_{x+1,y,z} + \text{H.c.}\right], \tag{S48}$$

$$\mathcal{H}_3(x,\ y,\ z) = \sum_{x,y,z} \left[\Psi^{\dagger}_{x,y,z} \left(-\frac{1}{2} s_z \sigma_z - \frac{i}{2} s_y \sigma_z - \frac{\Delta_0}{2}\sigma_x\right) \Psi_{x,y+1,z} + \text{H.c.}\right], \tag{S49}$$

and

$$\mathcal{H}_4(x,\ y,\ z) = \sum_{x,y,z} \left[\Psi^{\dagger}_{x,y,z} \left(-\frac{1}{2} s_z \sigma_z - i\frac{v_z}{2} s_z\right) \Psi_{x,y,z+1} + \text{H.c.}\right]. \tag{S50}$$

We now consider a 3D electric-circuit network forming a cubic lattice. The electric-circuit network consists of various nodes labeled by a. According to Kirchhoff's law, the current I_a entering the circuit at a node a equals the sum of the currents I_{ab} leaving it to other nodes or ground

$$I_a = \sum_b I_{ab} = \sum_b X_{ab}(V_a - V_b) + X_a V_a, \tag{S51}$$

where $X_{ab} = 1/Z_{ab}$ is the admittance between nodes a and b (Z_{ab} is the corresponding impedance), X_a is the admittance between node a and the ground, and V_a is voltage at node a. Using Eq. (S51), the external input current I_a and the node voltage V_a can be rewritten into the following matrix equation

$$\mathbf{I}(\omega) = \mathbf{J}(\omega)\mathbf{V}(\omega), \tag{S52}$$

where $\mathbf{I} = (I_1,\ I_2, \cdots,\ I_N)$, $\mathbf{V} = (V_1,\ V_2, \cdots,\ V_N)$, and N is the physical dimension. Here the $N \times N$ matrix $\mathbf{J}(\omega)$ is the circuit Laplacian, which can be used to simulate the system Hamiltonian $\mathcal{H}(\mathbf{k})$, having the form [6–8]

$$\mathbf{J}(\omega) = i\omega\mathcal{L}(\omega) = i\omega\mathbf{C} + \frac{1}{i\omega\mathbf{L}} + \frac{1}{\mathbf{R}}, \tag{S53}$$

where $\mathbf{C}$, $\mathbf{L}$ and $\mathbf{R}$ are the capacitance, inductance and resistance matrices, respectively.

To simulate the Hamiltonian $\mathcal{H}(x,\ y,\ z)$, we require $\mathcal{L} = \mathcal{H}$. Figure S4(a) plots the unit-cell circuit for the cubic lattice consisting of four nodes. Each node is connected to grounded electric elements for simulating the diagonal entries in the Hamiltonian $\mathcal{H}_1(x,\ y,\ z)$ in Eq. (S47). The on-site gain and loss are realized by the resistive elements R_A and R_B. The electric circuits for simulating Hamiltonians $\mathcal{H}_2(x,\ y,\ z)$, $\mathcal{H}_3(x,\ y,\ z)$, and $\mathcal{H}_4(x,\ y,\ z)$ are shown in Fig. S4(c-e). The inductors and capacitors between two neighboring nodes contribute hopping terms with positive and negative amplitudes [7], respectively. For the hopping with imaginary amplitude, we use a negative impedance converter with current inversions (INICs) [7], as shown in Fig. S4(b). When the current flows towards the INICs (the large arrow), the resistance is negative, and it is positive when the direction is opposite.

As indicated in the electric circuits in Fig. S4, the Laplacian that simulates the Hamiltonian $\mathcal{H}(\mathbf{k})$ in Eq. (1) in the main text reads

$$\begin{aligned}\mathcal{L}(\omega) = \ & \left(M_E - J_E\cos k_x - J_E\cos k_y - J_E\cos k_z\right) s_z\sigma_z + \left(v_E \sin k_z + i\gamma_E\right) s_z + t_{E1}\sin k_x s_x\sigma_z + t_{E2}\sin k_y s_y\sigma_z \\ & + \Delta_E\left(\cos k_x - \cos k_y\right)\sigma_x + i\lambda_E\mathcal{I},\end{aligned} \tag{S54}$$

where

$$M_E = C_1 = 1/(\omega^2 L_1),\;\; \gamma_E = 1/(2\omega R_B) - 1/(2\omega R_A), \tag{S55}$$

$$\lambda_E = -1/(2\omega R_B) - 1/(2\omega R_A),\;\; J_E = C_2/2 = 1/(2\omega^2 L_2), \tag{S56}$$

$$v_E = 1/(2\omega R_z),\;\; t_{E1} = 1/(2\omega R_x),\;\; t_{E2} = C_4/2 = 1/(2\omega^2 L_4),\;\; \Delta_E = C_3/2 = 1/(2\omega^2 L_3), \tag{S57}$$

and $\mathcal{I}$ is identity matrix. Note that the last non-Hermitian term does not change the topological features of the system. This electric circuit can be utilized to investigate the non-Hermitian higher-order Weyl-exceptional-ring semimetals studied in this work.

* These two authors contributed equally
† E-mail: yangzm@scut.edu.cn
‡ E-mail: fnori@riken.jp

[1] R. Jackiw and C. Rebbi, "Solitons with fermion number 1/2," Phys. Rev. D **13**, 3398 (1976).
[2] T. Helbig, T. Hofmann, S. Imhof, M. Abdelghany, T. Kiessling, L. W. Molenkamp, C. H. Lee, A. Szameit, M. Greiter, and R. Thomale, "Generalized bulk–boundary correspondence in non-Hermitian topolectrical circuits," Nat. Phys. **16**, 747 (2020).
[3] D. Zou, T. Chen, W. He, J. Bao, C. H. Lee, H. Sun, and X. Zhang, "Observation of hybrid higher-order skin-topological effect in non-Hermitian topolectrical circuits," arXiv:2104.11260 (2021).
[4] S. Liu, S. Ma, Q. Zhang, L. Zhang, C. Yang, O. You, W. Gao, Y. Xiang, T. J. Cui, and S. Zhang, "Octupole corner state in a three-dimensional topological circuit," Light: Science & Applications **9** (2020).
[5] C. H. Lee, A. Sutrisno, T. Hofmann, T. Helbig, Y. Liu, Y. S. Ang, L. K. Ang, X. Zhang, M. Greiter, and R. Thomale, "Imaging nodal knots in momentum space through topolectrical circuits," Nat. Commun. **11**, 4385 (2020).
[6] C. H. Lee, S. Imhof, C. Berger, F. Bayer, J. Brehm, L. W. Molenkamp, T. Kiessling, and R. Thomale, "Topolectrical circuits," Commun. Phys. **1**, 39 (2018).
[7] Y. L. Tao, N. Dai, Y. B. Yang, Q. B. Zeng, and Y. Xu, "Hinge solitons in three-dimensional second-order topological insulators," New J. Phys. **22**, 103058 (2020).
[8] J. Dong, V. Juričić, and B. Roy, "Topolectric circuits: Theory and construction," Phys. Rev. Research **3**, 023056 (2021).